Available online at www.sciencedirect.com
ScienceDirect
Journal of Catalysis 250 (2007) 41–54
JOURNAL OF CATALYSIS
www.elsevier.com/locate/jcat

Indirect assessment of unknown zeolite structures through inference from zeolite synthesis comparisons coupled with adsorption and catalytic selectivity studies

S.I. Zones [a,*], C.Y. Chen [a], A. Corma [b], M.T. Cheng [a], C.L. Kibby [a], I.Y. Chan [a], A.W. Burton [a]

[a] *Chevron Energy Technology Company, 100 Chevron Way, Richmond, CA, USA*
[b] *Instituto de Tecnología Química de Valencia (CSIC-Universidad Politécnica de Valencia), Valencia, Spain*

Received 8 February 2007; revised 3 May 2007; accepted 6 May 2007

Available online 27 June 2007

Abstract

This study focuses on an attempt to determine the internal pore architecture for two unknown zeolites through comparison with a selection of known zeolites. Unlike most studies, we also attempt to gain insight into structures by analyzing synthesis conditions. The details of structure-directing agents (SDAs) for zeolite formation and the inorganic context in which they do and do not work provide important data. In addition to synthesis comparisons, we show comparative adsorption data (2,2-dimethylbutane) and catalysis selectivity (methanol conversion and hexane cracking) for the unknown and selected known zeolites that should have relevant pore features. We focused on zeolites with large and intermediate pores, particularly with channel intersections, and those with portals opening into larger cavities. In these three analytical approaches, the unknowns IM-5 and SSZ-57 matched best as multidimensional 10-ring zeolites.

Keywords: Zeolite catalysis; Adsorption; Synthesis studies; IM-5; SSZ-57; ZSM-5; SSZ-58; SSZ-35

1. Introduction

Recent work in zeolite science has made impressive strides in the development of capabilities to determine the 3-dimensional structures of novel zeolites, even when crystallites are too small for single-crystal analysis. Most zeolites do indeed crystallize more in the micron and submicron range. The introduction of novel materials continues to expand rapidly [1], so the need for determination of pore architecture and potential for various applications remains high. Data analysis programs like ZEFSAII [2], FOCUS [3], XLENS [4], and other novel techniques combine diffraction data and computer modeling to assess how well trial structures can generate the experimental X-ray powder diffraction data. A recent diffraction analysis coming as a seminal breakthrough describes the structure solution of a material, TNU-9, that has the greatest number of unique symmetry tetrahedral atoms in the structure (22) of any material solved to date [5]. In the present work, we consider this material, with newly described structure, as part of the synthesis comparison data. Moreover, stretching out before us to the horizon is the knowledge that research groups of Treacy [6] and Deem [7] have been generating millions of hypothetical structures that could exist if conditions for their synthesis were found.

Despite the rapid growth in the number of new zeolite structures, now close to 175 (see the International Zeolite Association website at http://www.iza-structure.org), and in the ability to solve structures, some problems remain that are not readily solved. For example, there may be a mix of complex structures with numerous unique tetrahedral atom (T atom) sites, producing overlap in the diffraction peaks needed for analysis, and some materials may experience faults in growth, thus obscuring some lines in the powder patterns. The combination of better resolution of diffraction data (from synchrotron sources) coupled with clever computational tools like DIFFAx [8] can sometimes provide the means to solve structures of new materials that exhibit polymorphism. The solution to zeolite SSZ-26,

* Corresponding author.
E-mail address: sizo@chevron.com (S.I. Zones).

0021-9517/$ – see front matter
doi:10.1016/j.jcat.2007.05.005

the first known zeolite with both 10- and 12-ring apertures, was derived from this type of approach [9].

In the present study, we focus on two unsolved zeolite materials, IM-5 [10] and SSZ-57 [11]. Studies on IM-5 that combine catalysis screening reactions with some physical characterization methods have been reported previously [12–14]. *N*-decane hydroisomerization, *n*-hexane cracking with the use of *m*-xylene as a probe molecule, and microcalorimetric studies all indicated a type of 10-ring zeolite. These studies indicated that the zeolite could be a material with intersecting 10-ring pores or 10-ring channels that opened in to larger lobes between the channels [13a,13b]. Other studies have demonstrated a larger-pore zeolite [14]. We bring the analysis of synthesis into the picture here, noting for the first time that it is also an important tool in assessing zeolite structure. We rank the behavior of these zeolites against a suite of other known materials with features that may have some relationship with them.

Generally speaking, a survey of the zeolite catalysis literature over the last decade has shown us that where comparisons are made, four zeolite materials—Y zeolite (faujasite), ZSM-5, Beta, and mordenite—have received the most attention. These materials are all industrial catalysts available as manufacturers' samples, and they provide a range of active zeolite catalysts for comparison. Ferrierite is sometimes included in this list as well. Here we widen our net and look at a greater variety of structures, many of which need to be synthesized in the presence of organic guest molecules (SDAs).

To give an idea of the wide the variety of materials in terms of pore architecture that can be considered, we list roughly a dozen types in Table 1. For inclusion, the references are also provided. But our point of departure here is our examination of the synthesis of IM-5 and our use of some narrow compositional ranges for its synthesis. In contrast with several other zeolite syntheses, we show that there should be good prediction of the type of internal pore architecture that IM-5 should have. We follow up with some studies on the selective uptake of 2,2-dimethylbutane (with a kinetic diameter near 6 Å) from the gas phase and on the use of methanol as a feed under acid-catalyzed conditions, to examine the limitations on the size of aromatic products created, ranging from benzene to hexamethylbenzene. We assess pore size from the standpoint of what products can be made and then pass through the zeolite channels and out through the pores.

In this work, we use the IZA structure codes to describe the zeolites that we study, when such structures are known. We also provide representations of these structures in Appendix A.

Table 1
Representative high-silica zeolites which cover a variety of pore architectures

1. Large pore 1D	MOR	www.iza-structure.org
2. Large pore multi-D	FAU	www.iza-structure.org
3. Medium pore 1D	ZSM-48	[17]
4. Medium pore multi-D	ZSM-5 (**MFI**)	www.iza-structure.org
5. Small pore 1D	MCM-35 (**MTF**)	[15]
6. Small pore multi-D	SSZ-13 (**CHA**)	[16]
7. Medium pore 1D, large cavities	EU-1, SSZ-35 (**STF**)	[19]
8. Large pore and medium pore	SSZ-33 (**CON**)	[9]
9. Ultra-large pore	UTD-1 (**DON**)	[22]
10. Medium pore 1D with tortuosity	ZSM-23 (**MTT**) vs ZSM-48	[18]
11. Large pore with undulation	SSZ-42 (**IFR**)	[21]
12. Ultra-large pore & large pore	IM-12, ITQ-15	[23]
13. 18-ring by 10-ring	ITQ-33	[24]

2. Experimental

2.1. Zeolite synthesis

In this work, the typical synthesis of a high-silica zeolite involved combining a solution with a specific SDA, an alkali hydroxide, an aluminum source, and a silica source. In most of our reactions, we used the SDA as a quaternary ammonium hydroxide compound. For IM-5, we used the SDA as a bromide salt. The reaction mixture was then heated in a closed reactor (typically a Parr 4845 23-mL reactor type) while rotating on a spit within an oven. We followed literature procedures for the synthesis of zeolites. For large-pore zeolites, we synthesized zeolites SSZ-33 with Al replacing boron postsynthesis [25]. The SSZ-42 material was obtained from a combined Al, B synthesis [26], and SSZ-31 was obtained from patent examples [20,27]. Intermediate-pore zeolite ZSM-5 (**MFI**) was used as a commercial sample from Zeolyst. ZSM-11 (**MEL**) was prepared using the selective SDA of Nakagawa [28] and following the same inorganic procedures used to make SSZ-57 [11], so that these materials could be compared more directly. SSZ-58 (**SFG**) [29] and SSZ-35 **STF** [30,32] were prepared from patent examples. EU-1 (**EUO**) was prepared as reported in the literature [31]. Finally the synthesis of IM-5 was modified [13b] from the original patent [10]. The physical properties for these zeolites are given in Table 2.

2.2. Characterization

The as-made zeolites were washed and dried, then submitted for X-ray diffraction. A Siemens D-500 instrument was used for the measurements. Scanning electron micrographs were obtained using a JEOL field emission instrument (model JSM6700F). Our high-resolution electron micrographs

Table 2
Characterization of the zeolite samples made for this study

Zeolite	SiO_2/Al_2O_3	Crystal size (μm), aspect
IM-5	38	0.5, rectangular
Al SSZ-33 (**CON**)	36	0.5–2.0, cigar shaped
Al/B SSZ-42 (**IFR**)	80	0.5–1.0, pill shaped (tablet)
SSZ-31	80	0.5, thin rods
ZSM-5 (**MFI**)	40	0.5, polycrystalline aggregates
ZSM-11 (**MEL**)	55	0.3, spherical
SSZ-58 (**SFG**)	45	2.0–4.0, brick shaped
SSZ-57	55	0.5, spherical
SSZ-37 (**NES**)	80	1.0, brick shaped
EU-1 (**EUO**)	55	0.3, spherical

were obtained at Arizona State University's Center for High-Resolution Electron Microscopy; some of the protocol details have been published previously [33]. Detailed high-resolution microscopy analyses were carried out on JEOL 4000 EX instrument operating at 400 kV with a point-to-point resolution of <2 Å. The specimens were prepared by taking crushed zeolite powder and then dispersing it as thin sections over a holey carbon film supported on a copper grid.

The IR studies were carried out using a Nicolet Magna 550 FTIR spectrophotometer equipped with a KBr beam-splitter. The system used a DTGS detector and an ATR cell (from ASI) with a KRS-5 crystal giving useful spectra down to 350 cm^{-1}.

Materials were calcined for the removal of SDA molecules before the subsequent treatments. A program of heating at 1 °C/min to 120 °C (hold for 2 h), at 1 °C/min to 540 °C (hold for 5 h), and then at 1 °C/min to 595 °C (hold for 5 h) was used. The heating was conducted in flowing air with the zeolites thinly spread out on glass plates. The calcined zeolites were then given 2 ion-exchanges with ammonium nitrate in water. The typical procedure involved heating a 1/1 mass zeolite/exchange salt in 100× mass water in an oven at 90 °C for 2 h. This process was repeated twice, and then the product was collected on a filter and washed. This process was not carried out for Al-SSZ-33, the creation of which followed a different process [25]. Portions of the ion-exchanged zeolites were then recalcined (to the H^+ form) before any gas uptake measurements were made.

The gas uptake for nitrogen was measured using a Micromiretics 2100 instrument, and both micropore volumes and surface areas (BET method) were reported. For the materials for which argon data are reported, the analysis was carried out using a Coulter Omnisorp 100 CX instrument with measurements at −186 °C using both static- and continuous-flow techniques. Samples were first degassed in vacuo (below 10^{-6} Torr) at 300 °C for 2 h. Under continuous-flow methods, about 1000 data points were obtained for argon pressures ranging from 10^{-6} to 550 Torr. Sample sizes were typically 100 mg, and the flow rate was low enough such that the micropore filling capacities of the samples were usually reached in 1–2 h. Micropore volumes and external surface areas were taken from alpha-plot analyses of the adsorption isotherms. Alpha values were obtained from a silica standard (CPG-75) [34]. We previously described the use of the Cahn microbalance for measurement of hydrocarbon uptake for the determination of extra-large pore zeolites based on using tri-isopropylbenzene as an adsorbate [35]. The uptake analyses were obtained while the relative vapor pressure was maintained at $P/P_0 = 0.30$.

2.3. Catalysis

The methods that we used to study the conversion of methanol to hydrocarbons have been previously published and involve the use of a down-flow reactor, online gas chromatography (GC) with 6-port Valco switching valve, trap collection of liquids (in a cold bath of dry ice), and subsequent GC/MS analyses [36]. First, 0.50 g of zeolite (20–40 mesh) were loaded into a 3/8-inch stainless steel reactor for use in a Lindbergh furnace with thermocouple control of the reaction zone to within 10 °C. The catalyst was supported by a layer of acid-washed alundum above and another layer of glass wool below. The feed used in this study was 22% methanol in water, and the delivery was via a syringe pump at 1.59 cc/h. The temperature on the controller was set to 371 °C, and the outlet lines from the reactor were kept hot (204 °C) with heating tape and a controller. The HP 5880 GC was run blank between catalyst runs to ensure no heavy product carryover into the sampling lines from the previous run.

The GC/Ms analyses were made by taking the liquid product from the methanol conversion run and shaking and partitioning the material with an equal volume of dichloromethane. A 10-μL syringe was used to draw a sample from the dichloromethane phase. The sample was injected into a HP 5890 gas chromatograph equipped with a 60-m DB-5MS column. The system was interfaced with a HP 5970 MSD mass spectrophotometer with scanning from 40–800 daltons in 1 s. The GC temperature program was typically 0/0/5/320/5, and a 2-μL injection and a 100:1 split ratio was used. Compounds were checked against our internal library or against co-injected samples. The constraint index studies were carried out as previously described by Harris and Zones [37] also using a down-flow reactor, 0.50 g of 20–40 mesh catalyst, a 50/50 volume feed of *n*-hexane and 3-methylpentane, nitrogen carrier gas, and atmospheric conditions.

3. Results and discussion

3.1. Comparison concerning zeolite synthesis

The synthesis of IM-5 requires two interesting boundary conditions. That is not unusual but can indicate that for some key features in the structure, the correct synthesis conditions must be achieved. Our interest lies in investigating how the boundary conditions for the synthesis of a zeolite like IM-5 might help "narrow down" the possible solution candidates. Here we develop an analysis of (a) what might be eliminated as candidate structures and (b) what other zeolites with known structures have the same synthesis boundary conditions. To put this analysis in context, we first consider some generalizations about high-silica zeolite synthesis:

(a) Most high-silica zeolites require an organic guest to stabilize the internal space of the growing zeolite against an equilibrium event of redissolution. Over time, the guest usually has a good spatial fit into the open areas of the host zeolite. In other words, the guest organic cation fits the host inorganic lattice well, usually tightly enough to be trapped inside it. Only zeolites with a larger amount of Al in their framework, and the corresponding alkali cations associated with the framework anion charge, can grow and remain stable without an organic guest.

(b) The process of growing a zeolite appears to be under kinetic control. The small energy changes associated with the process [38,39] mean that in many instances, small changes in a set of conditions can lead to the formation

of other zeolites. Generally, very large organic guests have high selectivity for just a certain zeolite (e.g., the organocobalt compound in 14-ring UTD-1 synthesis [40]). Small guest molecules like tetramethylammonium have very little selectivity and can be found in a variety of zeolite preparations [41]. Occasionally a guest molecule has great selectivity for a certain zeolite host over a great range of conditions, but this remains an exception [42]. For example, as we discuss below, the SDA that makes IM-5 can do so only under certain reaction conditions.

(c) As the substitution for silica in the framework diminishes, zeolites with higher framework densities (i.e., more tetrahedral atoms per unit volume; an extreme boundary is the nonzeolitic phase quartz) are favored [43]. For a linear guest, if they are not too large in circumference, ZSM-48 becomes a default product. It is a one-dimensional 10-ring zeolite listed in Table 1. Many diamines and diquaternary ammonium compounds can be guest molecules in the synthesis of ZSM-48 once the Al substitution drops below 1 per 50 SiO_2. As the molecules become larger in cross-section or circumference, remaining much longer than wide, ZSM-12 (**MTW**) becomes favored. This latter material figures into our analysis. It is a one-dimensional, high-framework density material, but the pore is now a 12-ring structure (termed large pore).

(d) Conversely, zeolites that form best with some requirements for boron or aluminum in the framework (with Si/Al values in the range of 10–25) often have channel intersections in the internal pore structure. These can be continuous channels, as in ZSM-5 (**MFI**), or expanded cavities that connect via the channels, as in NU-87 (**NES**) [44]. Thus, with the backdrop of these several trends in creating high-silica zeolites, we proceed to a more detailed analysis of the synthesis of IM-5.

In the case of IM-5, we see two conditions of interest relative to the above arguments. The zeolite forms in a narrow Si/Al range, between about 15 and 25, and is formed from only one member of a series of homologous diquaternary compounds (see Fig. 1), for which only a certain length of molecule will work. The general structure of the diquaternary compound is shown in Fig. 1, which compares the zeolite products for the various chain lengths and in conditions of a synthesis where the reactant Si/Al synthesis ratio is either 17 or 33. Of the eight circumstances considered, only one produces IM-5. On the other hand, we can see that at lower Si/Al, more than one length produces Beta (BEA*), and all lengths produce the 12-ring zeolite **MTW** at high Si/Al. Of particular note is that when these latter two phases grow, they have continuous large pores. Thus, it is not surprising that the change in chain length connecting the centers where charge resides may not matter too much. We can see this trend in earlier data from the zeolite literature, where a smaller end group can allow ZSM-48 to form as the continuous channel product at high Si/Al (see Table 3). Certain "step-out" products are produced for which discreet chain lengths work but many do not work. This can be seen for EU-1 (**EUO**), which has 10 rings with certain side-pockets

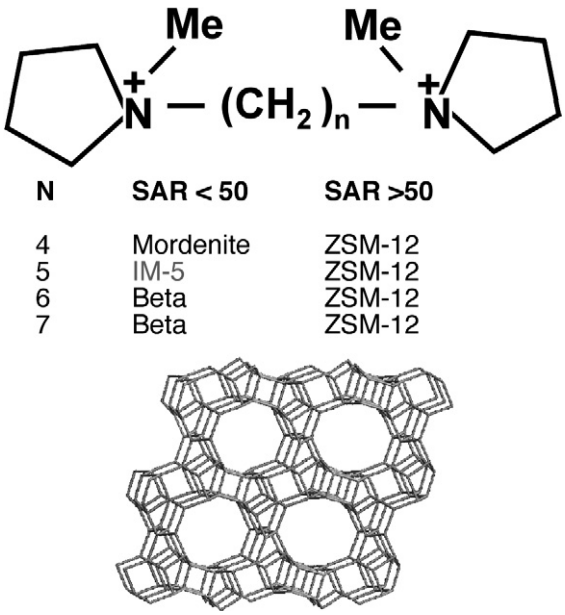

Fig. 1. Boundary conditions for making IM-5 at SiO_2/Al_2O_3 ratios above and below 50 (33, 66) and the effect of changing chain lengths between the two symmetrical charge centers. The structure of ZSM-12 (**MTW**) is shown as all the higher silica experiments make it regardless of chain length. Note that for $n = 4$ and SAR < 50, zeolites TNU-9 and TNU-10 can be made under different conditions than used here.

Table 3
Representative aluminosilicate phases obtained using $(CH_3)_3N^+(CH_2)_nN^+$-$(CH_2)_3$ as directing agent. Taken from results in the literature. See Ref. [18]

n	Si/Al[a]	Days	Temp. (°C)	Products
5	30	3	160	EU-1
	∞	4	160	ZSM-48
6	45	4	160	EU-1
	250	3	160	ZSM-48
7	45	3	160	ZSM-23
8	45	6	180	ZSM-23
	100	5	160	ZSM-48
9	45	6	180	ZSM-12
10	23	6	180	ZSM-12[b]
	45	5	180	NU-87
	90	3	180	ZSM-5
	∞	3	180	ZSM-48
11	45	6	180	ZSM-23
12	45	6	180	ZSM-23
	∞	3	180	ZSM-48
14	45	12	180	ZSM-12[c]
	45	5	180	ZSM-35[c]
16	45	10	180	ZSM-35

[a] Atomic mole ratios.
[b] K^+ substituted for Na^+.
[c] A secondary layered phase is also present.

off it [19b]; **NES** [44], with 10-ring pores connected by 12-ring segments internally; and **MTT**, with a one-dimensional 10-ring with a periodic corrugation in the pore walls, creating some tortuosity in the system [45]. Thus, when there is to be a periodic change in the internal intersection (or change in space) within a pore, SDAs with certain chain lengths work, whereas others do not. Details of the guest molecule must conform to the periodicity of the host lattice. Fig. 2 restates this condition for

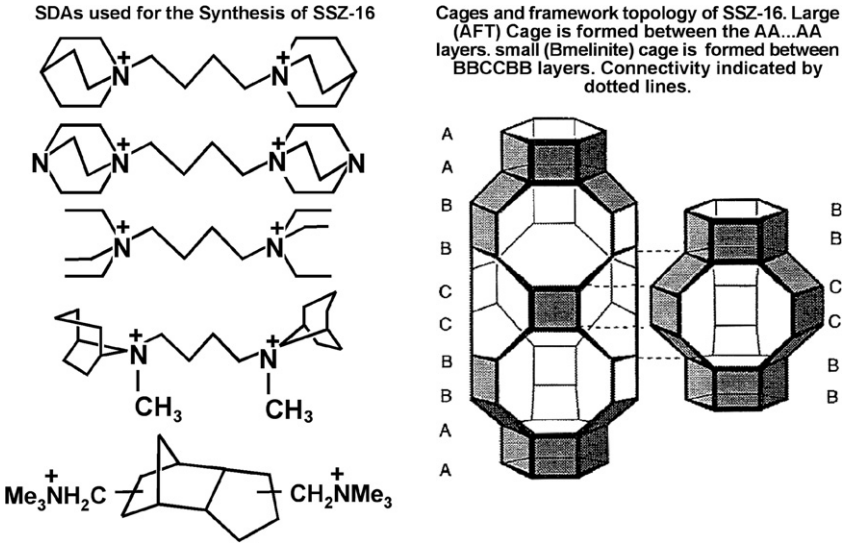

Fig. 2. A series of bulky diquaternary ammonium compounds which all make SSZ-16 (**AFX**) zeolite. They share a common feature that only with chain length = C_4 connecting the centers, is the zeolite made. The structure of the zeolite and the cages and stacking sequences which describe it are also shown. These large diquats fit lengthwise in the larger cage shown. Taken from Ref. [46].

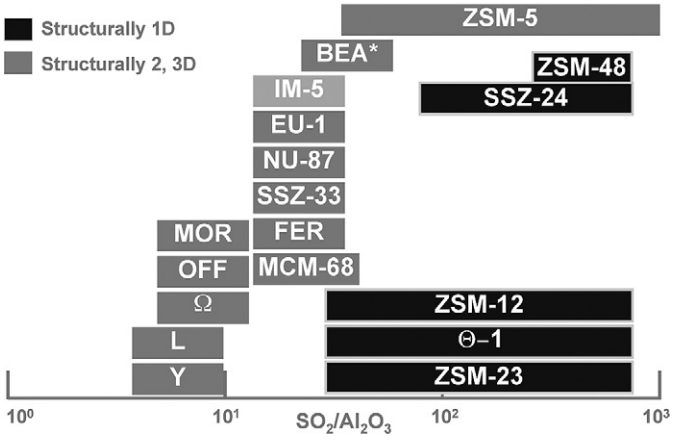

Fig. 3. A schematic representation of zeolite formation vs the SiO_2/Al_2O_3 boundary ranges where they are likely to form. Note that the 1D zeolite materials extend out into the range of no lattice substitution. IM-5 has a narrow range where it forms.

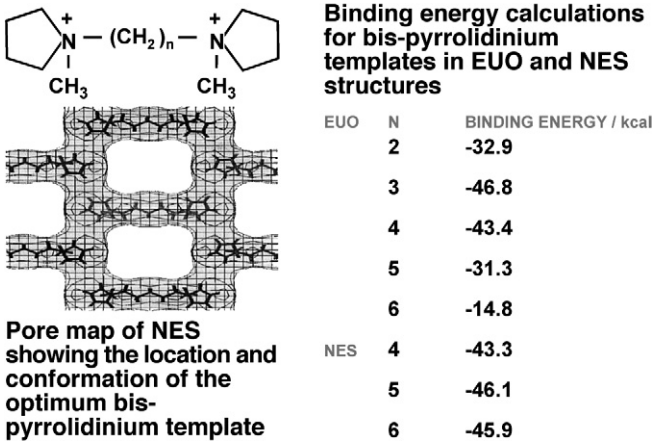

Fig. 4. A schematic of the fit of the IM-5 template into the pore segments in **NES**. Also shown for comparison are calculations for binding energies for inserting the different chain length templates (C_2–C_6) into either **EUO** or **NES**. The data is taken from Ref. [47].

an interesting related situation. Here a series of bulky loci for charge are separated by a chain length of C_4, and they all stabilize a certain large cage structure, zeolite SSZ-16 (**AFX**) [46]. Each locus has just the right length to fill this periodically restricted (i.e., with cavities connected by small pore windows) sequence of large cavities. Larger chain lengths typically lead to beta zeolite instead, with a continuous pore characterizing the host lattice. The periodicity is now lost. Beta is often the default structure that we see for linear SDA with bulky groups under lower Si/Al conditions; as we reported earlier, the complementary default for higher Si/Al will be **MTW**.

The issue of forming IM-5 in a narrow Si/Al range can be generalized to the series of zeolites plotted in Fig. 3. A number of other zeolites besides IM-5 are formed to the left (Si/Al on the x-axis), but not continuously out to higher Si/Al conditions. All of these materials with known structures have channel branching in their internal pore architecture. Meanwhile, there is also a series of products (e.g., **MTW**) that form only at the higher Si/Al end and have one-dimensional, nonintersecting channel systems. These form best as the lattice substitution diminishes.

Two other recent studies support this perspective on IM-5 having channel branching. One of these studies used the same series of SDA that we show in Fig. 1 [47]; surprisingly, under Si and Al conditions, IM-5 was not found, but after a switch to gallium from aluminum, **NES** zeolite was produced. The combination of synthesis data and molecular modeling led these investigators to believe that this SDA has a specific fit in the **NES** system (which is a 10-ring pore system connected between channels by 12-ring segments that do not run continuously). Fig. 4 shows their representation of how the molecule fits into the 10-ring (with 12-ring segments) structure.

Again, with reference to Fig. 1, the smallest chain length that we considered was C_4. We do not see IM-5, but instead get

MOR. In a study by Hong et al. [48] that used much greater amounts of Na cations, this C_4 SDA produced a novel high-silica version of stilbite (**STI**), a natural zeolite mineral, designated TNU-10. In that study, there is an intrusion of another unknown phase, seen much less often (but using the same C_4 SDA), referred to as TNU-9. Recently, a spectacular application of novel diffraction techniques and exhaustive computer processing allowed collaboration by the groups of McCusker and Baerlocher, Terasaki, Wright, and Hong (from whose lab the material originated) to solve this unusual structure [5]. The results of the study showed a structure of great complexity with a series of 10-ring aperture channels with pores running in all 3 directions of the zeolite. Again, the point to be made here is that the structure formed under narrow synthesis conditions and C_4 produces it but C_3, C_5, C_6, etc. do not. So there is a very selective fit as far as periodicity between points along a given channel, where there is a change in the dimensionality or details or along the pore. Our a priori assessment is that this should be true of IM-5 as well.

The arguments that we have presented earlier do not particularly apply to SSZ-57. Its synthesis relies on an SDA from a family for which nonsymmetric pyrrolidinium quaternary compounds have been prepared using enamine chemistry to react pyrrolidine with cyclic ketones. Following a reduction step, a further alkylation step introduces another substituent to complete the formation of the quaternary compound. In the synthesis of SSZ-57, cyclohexyl is the cyclic ketone and butyl is the last added group. **SFG** uses the same chemistry, the same last group and the cyclic center is cyclooctyl. While the size of the particular groups formed around the pyrrolidine is vital to the specification of the product SSZ-57, there is not the narrow inorganic chemistry for formation as seen for IM-5. It also is not entirely clear how the SDA fits into SSZ-57. Solving the structure of SSZ-57 will provide valuable information here. We included this unknown zeolite in this study because we believe the adsorption and catalysis studies that follow also shed important light on the possible structure.

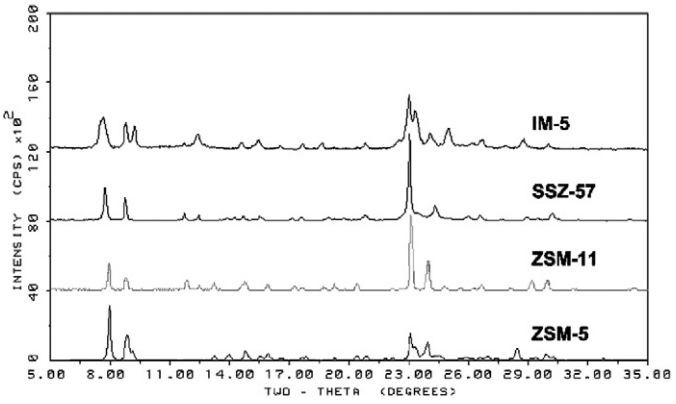

Fig. 5. XRD powder diffraction patterns of four zeolites in this study.

3.2. Characterization by physical methods

Some preliminary characterization of the new zeolites, SSZ-57 and IM-5, allowed us to see their potential relationship to the known and well-studied multidimensional 10-ring zeolites **MEL** and **MFI**. Fig. 5 compares the XRD patterns for all four materials; certainly, numerous similarities can be seen. From both the powder diffraction data and the TEM and HRTEM data, some unit cell parameters can be gathered. In some instances, the unit cell dimensions for the unknown materials have some relationship to **MEL** or **MFI**. For instance, SSZ-57 has 2 unit cell parameters equivalent to those of **MEL**; however, the value in the *c* dimension is longer in SSZ-57. (Below we discuss that there is support for a larger unit cell in the subsequent experimental work). Fig. 6 shows two HRTEM images for the two unknown zeolites, in which the appearance of orderly micropores can be seen. Other projections (not shown) give a picture of pores running in more than one direction.

An approach seldom used in comparing zeolites is the comparison of IR lattice patterns. Fig. 7 shows how similar the four

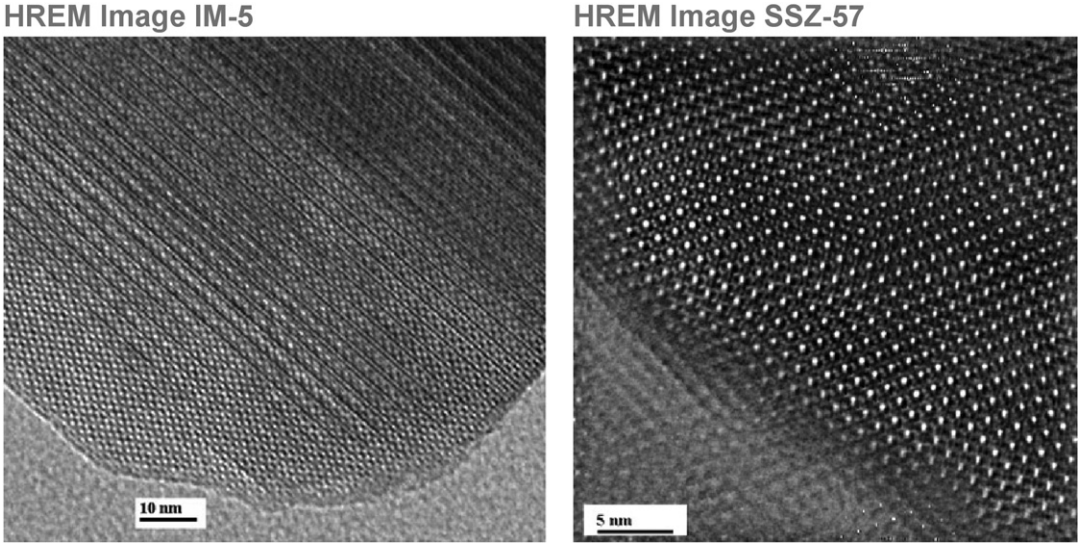

Fig. 6. High resolution electron micrograph images for unknown SSZ-57 and IM-5. At these high magnifications one can see the symmetric periodic pore apertures of the crystals seen at the outermost edges where there is a thin cross-section region.

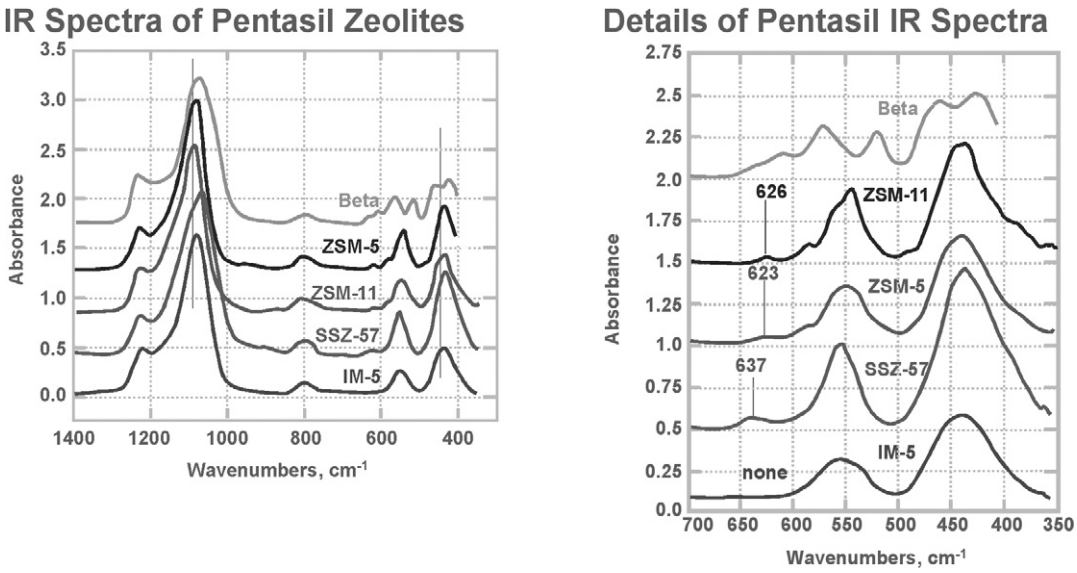

Fig. 7. Infrared spectra taken on the 4 related zeolites as pressed thin wafers. Two ranges are shown and some detail for beta zeolite is also given to show the pronounced difference in this spectra vs the other 4.

Table 4
Micropore volumes in cc/g nitrogen for the range of zeolites used in this study

Zeolite	Dimensions	N_2
ZSM-5 (**MFI**)	Multi-D	0.17
ZSM-11 (**MEL**)	Multi-D	0.17
NU-87 (**NES**)	10 with 12 cavities	0.18
EU-1 (**EUO**)	10 with 12 pockets	0.16
SSZ-35 (**STF**)	10 with large cavities	0.18
SSZ-58 (**SFG**)	2D10	0.18
SSZ-42 (**IFR**)	1D12	0.20
SSZ-31	1D12	0.11
IM-5	?	0.17
SSZ-57	?	0.17

materials are in terms of bands in the IR; for comparison, a pattern for BEA* is shown to indicate how there can be noticeable differences even though the BEA* is of comparable Si/Al value.

Along with the physical characterization via diffraction, useful information about the zeolites can be gathered by looking at adsorbate interactions. In the first instance, we show the micropore filling by nitrogen. Table 4 compares the data for the 2 unknowns and then the other 8 zeolites that we use as our collection of useful comparison materials. **IFR** and **CON** are large-pore zeolites; the latter has both 10- and 12-ring channel systems. SSZ-31 has a large pore, but it is a series of parallel one-dimensional pores with no variation in the walls. We have already alluded to the comparison of the 2 unknowns to **MEL** and **MFI** as intersecting 10-ring systems. The new zeolite SSZ-58 (SFG) also has this feature, with pores slightly larger than those of **MFI** [49], so it is included. Then there are 3 materials where 10 rings in the structure open into larger regions formed by either side pockets (**EUO**), connecting 12-ring spacers (**NES**), or a large periodic cavity with only a one-dimensional set of 10 rings providing egress (**STF**). Looking at the data in Table 4, there is only one low-volume outlier. SSZ-31 has a value of 0.11 cc/g, whereas all of the other materials with known and unknown structures have values closer to 0.17 cc/g or higher. SSZ-31 is the only material in the group with a known one-dimensional channel system in which there are no interruptions in the internal geometry of the pore; no other pores intersect. Thus, it has a high framework density (as zeolite structures go) and lower internal void space.

Table 5
A comparison of organic pore-filling in the as-made zeolites, the available microporosity determined by argon (after removal of the organo-cations by calcination up to 600 °C) and the pore details for known structures

Zeolite	%Sum C, H, N	Pore filling, argon	D
SSZ-33 (12 × 10) (**CON**)	18%	0.20 CC/GM	3D
ZSM-5 (**MFI**)	12%	0.13	2D
ZSM-23 (**MTT**)	9%	0.10	1D
SSZ-42 (**IFR**)	16%	0.20	1D
SSZ-13 (**CHA**)	20%	0.32	3D
IM-5	12%	0.13	?

This set of comparisons already argues (as we did earlier) that IM-5 and SSZ-57 are not likely to be one-dimensional zeolites with either intermediate (10-ring) or large (12-ring, such as SSZ-31) pores. It is sometimes useful to compare the amount of organic material found in the pores of the guest/host product. The organic will have a relationship to the void volume found once the pores are emptied of the guest. Table 5 compares some of the zeolites listed in Table 4. Along with the carbon, hydrogen, and nitrogen values (wt%) found in the pores, the table gives the argon pore-filling values. In this analysis, a material like IM-5 is close to **MFI** in both facets. The values are lower than those for a 12/10-ring pore system, as seen in SSZ-33 (**CON**).

A further set of comparisons for the unknowns and **MEL** and **MFI** was carried out using a dynamic argon pore-filling approach. The plot of uptake versus partial pressure shows a remarkably similar profile for the four zeolites. The shift in the peak position to slightly higher partial pressure indicates

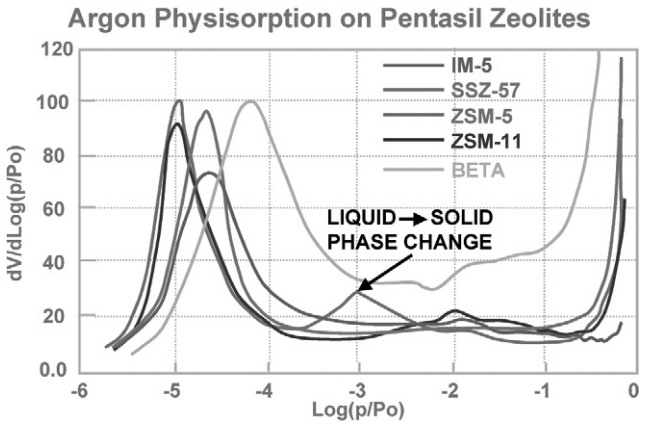

Fig. 8. Derivative plots of argon pore-filling vs partial pressure. The unknown SSZ-57 and IM-5 are slightly shifted to higher partial pressure maxima relative to **MFI** and **MEL**. But the shift is not so large as what is seen in beta zeolite (and other large pore zeolites).

a slightly larger gas-filling space in the internal architecture. Large-pore zeolites like BEA* (shown in Fig. 8) shift to even higher partial pressures. The data here argue away from either SSZ-57 or IM-5 having a continuous large pore that communicates with the exterior.

3.3. Characterization by hydrocarbon uptake; 2,2-dimethylbutane

In characterizing novel zeolites, before we know the structure, hydrocarbon uptake can be a valuable tool for assessing (1) the size of hydrocarbon that can enter the pore system, (2) the amount of pore filling, and (3) the uptake rates. This information provides insight into the structural features of the void region of the zeolite. For example, in previous work, one of the most fascinating examples that we encountered was this analysis on zeolite SSZ-25 (**MWW**) structure. We found high values for *n*-hexane uptake and much lower values for the uptake of larger adsorbates cyclohexane and 2,2-dimethylbutane. The *n*-hexane indicated that we had a material with larger capacity than one-dimensional pores. But it also indicated that there were limits to where other adsorbates could go in the structure. Only later when the structure was determined was it evident that there were 2 entirely noncommunicative 10-ring channel systems in the zeolite [50]. This structure emerged as one of the most complex to be synthesized, but the value of the uptake analysis had been nicely demonstrated.

Using a Cahn microbalance and operating under reduced pressure, we evaluated the rate and capacity for hydrocarbon uptake of IM-5. Fig. 9 shows the uptake curves over several hours for *n*-hexane (rapid), cyclohexane (gradual), and 2,2-dimethylbutane (slower yet). For an open 12-ring zeolite like **FAU**, Fig. 9 shows very rapid uptake for 2,2-dimethylbutane when the pores are of this size and the zeolite is multidimensional. These data show that IM-5 is not likely to be large pore unless there is only slow diffusion through a single-pore system. The rapid uptake of *n*-hexane and the magnitude of the uptake do not support this position, however.

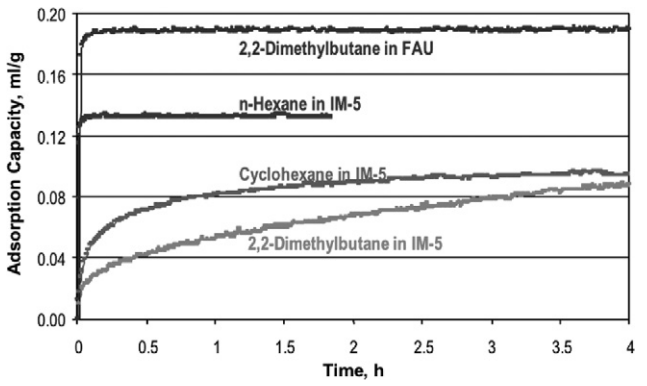

Fig. 9. Uptake profiles for hydrocarbon adsorbates on IM-5. See the text for details of the experimental procedure. One can see that the rate to reach a maxima and level off, becomes slower as the adsorbates increase in size for hexane compounds, *n*-hexane, cyclohexane and 2,2-dimethylbutane. For comparison, we show that the largest molecule experiences no slowdown for uptake when **FAU** (3D large pore) zeolite is tested.

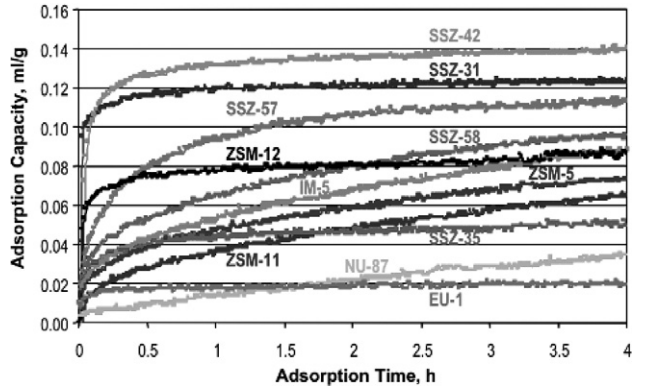

Fig. 10. Adsorption data profiles for 2,2-dimethylbutane uptake for several zeolites in this study. One can see how the rates are steepest for the large pore zeolites and then the 10-ring zeolites show a gradation of uptake rates. The smaller aperture 10 rings of EU-1 seem too small for uptake of this adsorbate at room temperature.

We then decided to look at the behavior of our suite of zeolite types under the same test conditions for 2,2-dimethylbutane (a diameter of nominally 6.2 Å, which is larger than the crystallographic pore size of almost any 10-ring zeolite). Uptake curves for the first 4 h of adsorbate exposure are plotted in Fig. 10. It can be seen that the most rapid pore filling occurs for the known large-pore systems SSZ-31 and SSZ-42 (**IFR**). The 12-ring (but hindered) **MTW** also shows a rapid uptake rate, but a lower overall uptake value. On the other hand, the 10-ring zeolites **EUO** and **NES** (even though they open into larger cavity regions) struggle to take up the adsorbate. The crystallographic 10 rings for **EUO** and **NES** are in fact smaller (**EUO**, 5.4 Å by 4.1 Å and **NES** 5.7 Å by 4.8 Å) than the other 10-ring zeolites in our study. **MFI**, **MEL**, **SFG**, and **STF** all have apertures with no cross-section minima below 5.1 Å.

For the unknowns, SSZ-57 and IM-5, we wanted to be able to compare them on some ranking parameter for the comparative uptake. Therefore, we created a value of $\mathrm{AI} = (t2/3)^{-1}$ wherein we ask the question as to when 2/3 of the uptake seen

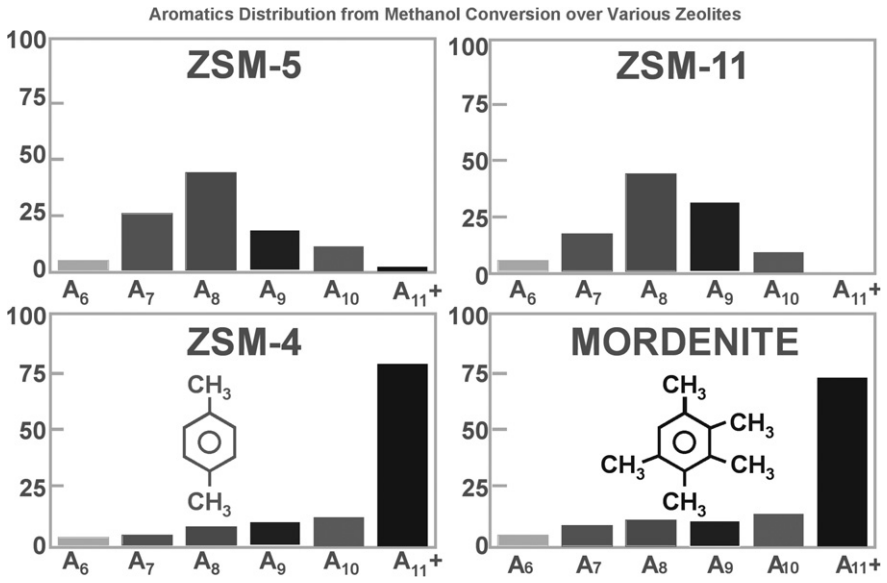

Fig. 11. Distribution of aromatics in the conversion of methanol. The data is taken from Ref. [54]. Each group in the histograms is built upon a single aromatic ring. Note that the large pore zeolites favor the larger product formation over the xylenes which dominate for ZSM-5 and ZSM-11. Two product structures (A8 and 11) are shown for guidance.

Table 6
Relative uptake of 2,2-dimethylbutane at room temperature The comparative rate is defined as looking at the time needed to achieve 2/3 of the uptake that will be measured out to 4 hours, as an inverse function[a]

Zeolite 22DMB	Rate of uptake	Zeolite 22DMB	Rate of uptake
ZSM-5 (**MFI**)	3.0	SSZ-58	5.0
ZSM-11 (**MEL**)	2.6	SSZ-42	16.0
NU-87 (**NES**)	2.0	SSZ-31	16.0
EU-1 (**EUO**)	0.0	IM-5	3.5
SSZ-35 (**STF**)	8.0	SSZ-57	8.0

[a] $(t_{2/3}$ uptake$)^{-1}$ over 4 h time period occurs.

over this 4-h time period occurs. We treat the numbers in an inverse fashion to create large numbers for fast uptake. For example, looking at the data in Fig. 10, it becomes apparent that the 2/3 uptake point for the large-pore zeolites occurs in a matter of minutes. The same treatment yields values in hours for most of the other zeolites in the group. We rank these uptake determinations in Table 6; as shown, IM-5 is closer to the **MFI**, **MEL** grouping and not as large as **SFG** or SSZ-57. This once again supports that the unknowns are more consistent with 10-ring zeolites. It will be interesting to test the novel three-dimensional 10-ring TNU-9 in such a test to see whether the uptake rates are affected or whether the entrance will remain slow due to pore size limitations.

In a more detailed study, we also investigated the effect of crystallite size as a factor in these rates [51]. Other studies, using the same equipment described here, measured uptake on the surfaces of zeolites in which the pores were still filled with SDA. We found a small but measurable uptake (in a matter of min) for crystallites like those for SSZ-32 (**MTT**) where the size of the zeolite crystals has a mean near 0.2 μm. The value does not change once the pores are open, because the 10-ring is too restricted and the pore system is one-dimensional. A similar analysis had been reported from this lab, using azoalkane dyes as adsorbate rate probes [52]. When the zeolite is capable of admitting 2,2-dimethylbutane then crystallite size can be a contributing factor for rate. This was shown previously for **MFI** [53]. Even with this additional complexity, we can see that, even given some differences in crystallite size among the 12-ring zeolites, all give much steeper uptake curves than the remaining mix of known and unknown materials. The utility of the method is demonstrated even if the rate determinations will be altered by this factor. The various crystallite sizes for the zeolites used in this study, determined from SEM, are given in Table 2.

3.3.1. Catalysis

Although we have probed the potential shape selectivity of this suite of zeolites by looking for adsorption selectivities, our goal is to understand the structures of unknowns IM-5 and SSZ-57. Traditional shape-selective catalysis is generally ascribed to three operating factors. There can be shape-selectivity based on which reactants can get into the interior of the zeolite. There is also a shape-selective factor in what transition states are possible (sterically) in confined spaces of zeolite pores. There can be selectivity where differential diffusion of products may be an important factor. We decided to examine the differential product behavior for these zeolites when reactions begin with a small molecule and increasingly larger products can be formed. The conversion of methanol to gasoline is a well-known zeolitic process and was a major triumph of new material use and chemical engineering at its inception [54]. Fig. 11 shows a histogram for aromatic selectivity observed by Chang et al. at Mobil [54] as they evaluated the impact of pore size on products made. Shown in the composite is that the large-pore (12-ring) zeolites like Mordenite and ZSM-4 (**MAZ** type) will make larger

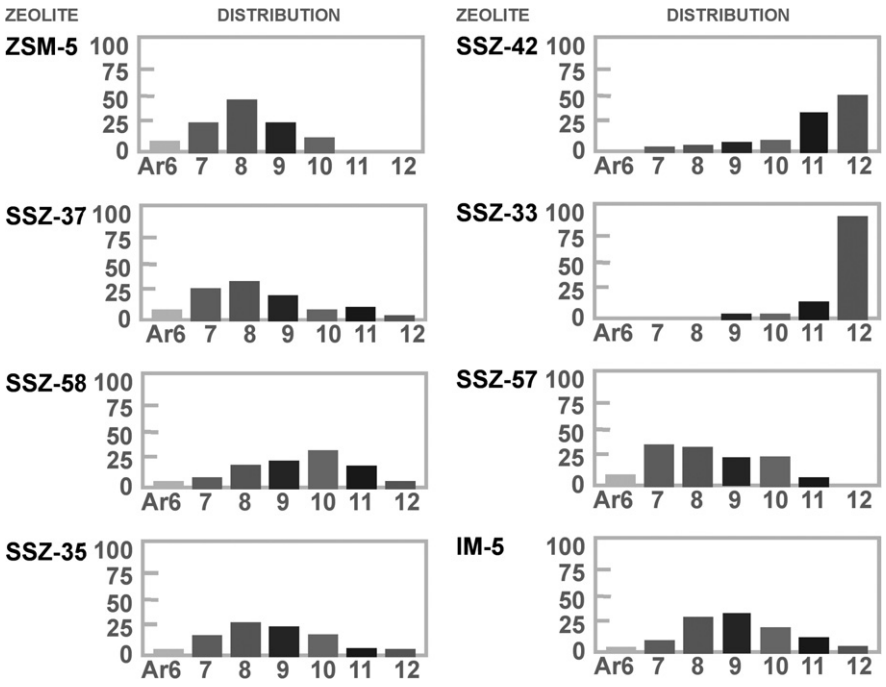

Fig. 12. Distribution of aromatics in the conversion of methanol for 8 of the zeolites used in our comparative studies relative to unknown SSZ-57 and IM-5. Large pore zeolites SSZ-42 and -33 again show products skewed towards the heavy A12 region (mostly hexamethylbenzene). The other 6 zeolites show very little A12.

aromatic molecules like penta and hexamethyl benzene while shrinking the product pool for lighter (usually more desirable) aromatics. Conversely, ZSM-5 and 11 (**MFI** and **MEL**) give a maximum product yield at the C_8 products (3 xylenes and ethylbenzene). If larger products like naphthalenes are made (which they are, as we discuss below), they will take much longer to emerge from the pore systems of the intermediate pore zeolites.

We ran the test as a down-flow reaction with our feed diluted with water. (The reaction has a sizable exotherm associated with it and produces water as a 56 wt% product anyway.) We previously compared the effects of acid strength for small- and large-pore isostructural sieves, varying from Si/Al to SAPO to borosilicates [36], using this approach. Products were identified by online GC, and a trap was used to collect liquid product (our aromatics) for further analysis. These collected liquids were subsequently analyzed by CG/MS to gain more detail on the heavier products made (e.g., dimethyl naphthalenes and substituted indanes). Some of the catalysts fouled with time on stream (in contrast with **MFI** and a few other zeolites); thus, we are looking at the GC data for 100% conversion before any methanol breakthrough is seen.

In a manner comparable to Chang's approach, Fig. 12 gives histograms for 8 of the zeolite systems investigated here. Two features are apparent. The large-pore zeolites (**CON** and **IFR**) give the heavier C_{11} and C_{12} products in much larger quantity than the other catalysts. An interesting feature here is that even though the formation of a pentamethylbenzene product might be expected to experience considerable steric hindrance over a trimethyl derivative, there seems to be ring induction such that each incoming group is activating the ring for further addition. The exact mechanistic mode of growth remains a subject of much research [55,56]. The second feature is that the unknowns IM-5 and SSZ-57 exhibit a shift toward C_9 in the products made, but they still seem to behave consistently in the camp of 10-ring zeolites as far as minimizing the C_{11} and C_{12} fractions formed. Along with **STF** and **SFG**, the IM-5 and SSZ-57 seem to shift to higher aromatic numbers compared with **MEL** and **MFI**. This may indicate larger pore openings (**STF** and **SFG**) even though they are still 10-ring, or a larger internal space off the incoming 10-ring, which might be true for SSZ-57.

We determined that one more comparison was warranted, going back to what was learned in the synthesis studies. We had found that only a certain chain length worked to make IM-5, and that if the Al content diminished, then **MTW** became the default structure. The **MTW** is a 12-ring one-dimensional zeolite, so the SDA can specify a 12-ring (rather than ZSM-48 as a 10-ring), and all chain lengths in the study can make the ZSM-12. It has a cross-section of closer to 6 Å and is one of the most hindered 12-ring zeolites, and thus is a good candidate for testing what happens with the aromatic selectivity in our test reaction. Fig. 13 replots the histogram data for IM-5 with ZSM-12 also included. We can see that even for this hindered 12-ring, with puckering of the pore mouth, it still makes the large aromatics seen by the other large-pore zeolites. Thus, even if IM-5 were to accommodate sections of a pore that were 12-ring in detail, like **NES**, then this 12-ring aperture would seem to not extend throughout the pore system to reach the external surface.

Previous studies on these materials have focused on a various catalytic tests. Corma et al. [13] used xylene isomerization and isomerization versus disproportionation reactions to assign IM-5 as an intermediate-pore zeolite when ranked against some

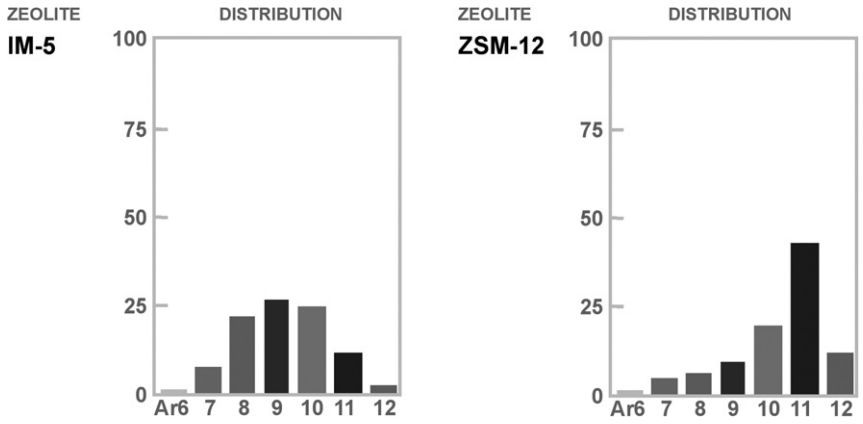

Fig. 13. A direct comparison of the aromatics formed from methanol using zeolites IM-5 and ZSM-12 as catalysts. ZSM-12 is the default crystallization product for all the chain lengths we employed (Fig. 1) as the SiO_2/Al_2O_3 ratio is higher. ZSM-12 is considered a "puckered" 12-ring and does not have as large a cross-section as most 12 rings. It still produces a maximum at A11 which is noticably larger than what is seen for IM-5.

other zeolites. Using *n*-octane at 900 °F, Bong et al. considered IM-5 to better correspond to a multidimensional large-pore zeolite [14]. Other test reactions have been developed with an interest in determining the internal void space details of zeolites. One can argue that use of tests like the spaciousness index [57] (a hydrocracking of a model feed) or the propene alkylation of toluene [58] (iso/*n* ratio for the propyl substituent) would have been useful for these studies as well. We had also invested in understanding a reactant shape-selective catalytic cracking reaction, the constraint index (CI), developed at the Mobil labs a few decades ago [59]. This test is a cracking reaction with equal volumes of *n*-hexane and 3-methylpentane feed. The concept is that restricted pores should be more selective (reactant shape selectivity) toward cracking of *n*-hexane. In the absence of a restriction (i.e., a large pore), there should be equimolar conversion. But the cracking reactivity of the branched isomer is greater, so in fact it can be preferred in the absence of constraints. This translates into CI values <1 for active, large-pore zeolites. Very constrained 10 rings like SSZ-32 (**MTT**) give values above 12, with a great preference for cracking *n*-hexane. Table 7 shows a series of runs (some taken from our previous study [37]), listing the unknowns IM-5 and SSZ-57. Once again, the cracking data show a preference for the *n*-hexane over the 3-methylpentane, demonstrating that there is constraint in the pore system over an open 12-ring portal of the type described previously [14]. (An additional caution about the evaluation of IM-5 is that there is some uncertainty about the presence of small impurities in the synthesis products. In hindsight, the materials that we have from 3 different labs may contain small amounts of TNU-9, the structure of which has been described only recently [5]. Nonetheless, the behavior of our samples of IM-5 in adsorption studies or catalysis places it in the category of containing intermediate pore apertures.)

Table 7
Constraint index measurements (see text for definition) for a variety of zeolites. The zeolites are ranked by selectivity for hexane over 3-methylpentane, with the two unknowns at the bottom of the table. Also shown is the relative product distribution of iso/normal butanes made. This ratio is a good indicator of large cavities within a structure. Compare ZSM-5 with all the other zeolites in the table below it (SSZ-23 is restricted by 9 rings)

Structure	Temp. (°C)	Feed conv. (%)	CI	I-C_4/*n*-C_4
SSZ-13 (**CHA**)	371	16.9	>100.0	0.14
ZSM-23 (**MTT**)	427	37.2	10.6	0.69
SSZ-20 (**TON**)	427	54.7	6.9	0.59
ZSM-5 (**MFI**)	316	71.6	6.9	1.31
SSZ-28 (**DDR**)	427	12.3	4.0	1.07
EU-1 (**EUO**)	427	89.3	3.7	2.26
ZSM-12 (**MTW**)	371	96.1	2.1	2.51
SSZ-23 (**STT**)	427	6.0	3.2	0.70
SSZ-36 (**ITE/RTH**)	371	49.5	1.1	3.90
SSZ-31	427	67.0	0.9	3.72
SSZ-25 (**MWW**)	316	98.9	0.8	4.20
SSZ-35 (**STF**)	316	94.9	0.6	3.41
LZY-82 (**FAU**)	316	82.9	0.4	5.97
CIT-5 (**CFI**)	427	38.1	0.4	3.59
SSZ-24 (**AFI**)	371	83.4	0.3	5.49
UTD-1 (**DON**)	371	74.6	0.3	5.97
IM-5	316	80.0	1.8	4.00
SSZ-57	316	78.0	1.1	3.50

4. Conclusion

An effort was made to characterize two new high-silica zeolites by combining a specific adsorption and catalysis test, and then studying various other, newer zeolites that have relevance in this situation. We chose zeolites SSZ-35 (**STF**), SSZ-58 (**SFG**), EU-1 (**EUO**), and NU-87 (**NES**) as unusual materials that have intermediate-pore boundaries that open into larger spatial regions within the zeolite. Well-studied zeolites like ZSM-5 (**MFI**) and ZSM-11 (**MEL**) were also included. In addition, in the case of unknown IM-5, an analysis of a number of related synthesis systems was carried out to gain insight into the likely pore structure, given the details of the SDA used and the inorganic boundary regions. This approach, rarely used in the analysis of unknown zeolites, proved quite useful.

As shown by the measured uptake rates for 2,2-dimethylbutane, the unknown zeolites IM-5 and SSZ-57 better fit into the category of materials bounded by 10-ring apertures. Once

again, a wide range of materials was studied, and the uptake rates were considerably faster for the 12-ring zeolites. We did find rapid *n*-hexane rates for IM-5, indicating an absence of pore blockage leading to hindered uptake of 2,2-dimethylbutane.

The model reaction that we used in the catalysis comparisons was the conversion of methanol to aromatic hydrocarbons. Olefins and alkanes are formed as well, but we focused on the size distribution of the aromatic molecules as an indicator of the types of products that can be made internally and escape the pore system. We found that large-pore zeolites give considerably more C_{11} and C_{12} aromatics than the intermediate-pore zeolites in which the structures are known. Based on our results, the unknown zeolites IM-5 and SSZ-57 fall into the category of intermediate-pore zeolites, even though they have product distributions that appear larger than those for ZSM-5 (**MFI**) reported in the literature and our results here. In the case of IM-5, this catalysis result is in line with results reported by Corma et al. [13]. Our CI evaluation also produces an IM-5 catalyst that, although indicative of intermediate pore behavior, seems less selective than **MFI**. SSZ-57 seems to be less selective than **MEL**, with which it surely has a structural relation.

Finally, it is worth noting that the best way to use the techniques that we discuss in this analysis is in combination. For example, dimethylbutane uptake studies can carry concerns about rates being affected by crystallite size, particularly for one-dimensional zeolites. In this study, most of the materials used had relatively small crystals (<1 μm). The studies of product selectivity using the conversion of methanol to aromatics also can be influenced by how much external surface is available. We already stated that crystals were small for the most part, and Jones et al. [60] previously showed that aromatics like xylene can experience surface isomerization. Thus, the exact distribution of isomers in a given molecular weight group could be affected in this way. But the important result to note is that where there is a trend of pore size in terms of uptake for 2,2-dimethylbutane, when we look at the methanol conversion data, those same trends fall into place. There are no reversals of performance. This indicates that some of the issues that we raise here have little impact on the zeolite behavior in these tests.

Note added in proof

After we submitted our work, the structure of IM-5 was published in the open literature [61]. The material, which has a very complex structure, does in fact contain intersecting 10 rings defining the portal boundaries and configurations. This zeolite is one of the most complex seen to date and the groups of McCusker and Hovmoller have combined efforts and introduced some exciting new approaches to diffraction data analysis, showing remarkable creativity in defying the obstacles imposed on the possibility of structure elucidation in this problem where the unit cell is very large.

Acknowledgments

The authors thank their colleagues at Chevron's Energy Technology Center for support work. Bowman Lee and Tom Finger were instrumental in running our methanol conversion reactor studies. Jim Hudson assisted in the follow-up GC/MS analyses. Our high-resolution images of the two unknowns were produced at the Center for High-Resolution Electron Microscopy at Arizona State University in collaboration with Dr. Peter Crozier. Dr. Saleh Elomari provided the zeolite samples SSZ-57 and 58. The SEM images used for determining the crystallite size of our materials (Table 2) were collected by Tom Rea and Glenn Menard. Dr. Lynne McCusker (ETH Zurich) provided some useful comments in the revision stages of this manuscript.

Appendix A. Representations of the structures for the spread of material in this study

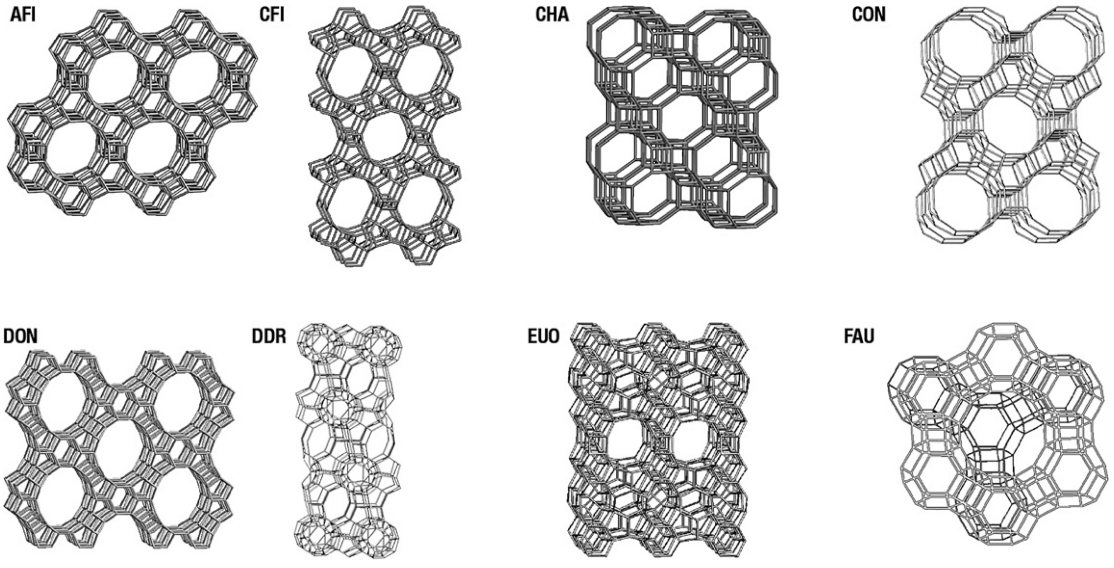

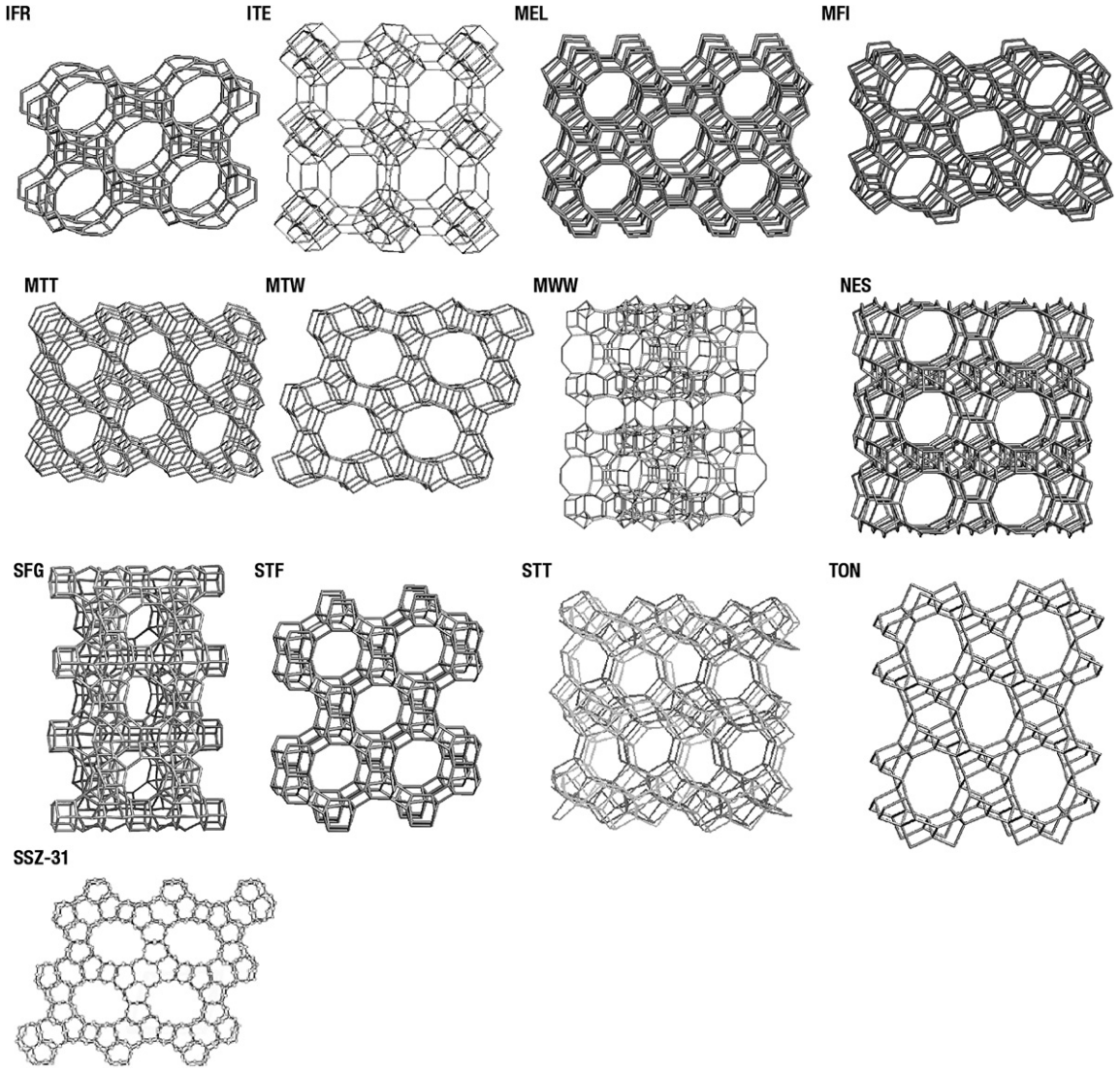

References

[1] S.M. Auerbach, K.A. Carrado, P.K. Dutta, Handbook of Zeolite Science and Technology, Marcel Dekker, New York, 2003.

[2] M.G. Wu, M.W. Deem, S.A. Elomari, C.Y. Chen, R.C. Medrud, S.I. Zones, T. Maesen, C.L. Kibby, I.Y. Chan, J. Phys. Chem. B 106 (2002) 264–270.

[3] R.W. Grosse-Kunstleve, L.B. McCusker, C. Baerlocher, J. Appl. Crystallogr. 30 (1997) 985.

[4] (a) J. Rius, Z. Kristallogr. 219 (2004) 826–832;
(b) A.W. Burton, Z. Kristallogr. 219 (2004) 866–880.

[5] F. Gramm, C. Baerlocher, L.B. McCusker, S.J. Warrender, P.A. Wright, B. Han, S.B. Hong, Z. Liu, T. Ohsuna, O. Terasaki, Nature 444 (2006) 79.

[6] M.D. Foster, M.M.J. Treacy, Atlas of Prospective Zeolite Frameworks; http://www.hypotheticalzeolites.net.

[7] D.J. Earl, M.W. Deem, Ind. Eng. Chem. Res. 45 (2006) 5449–5454.

[8] M.M. Treacy, J.M. Newsam, M.J. Deem, DIFFaX Version 1.801 (1995).

[9] R.F. Lobo, M. Pan, I.Y. Chan, R.C. Medrud, S.I. Zones, P. Crozier, M.E. Davis, J. Phys. Chem. 98 (1994) 12040–12052.

[10] E. Benazzi, J.-L. Guth, L. Rouleau, US Patent 6,136,290 (10/24, 2000).

[11] S.A. Elomari, PCT US02/21172 (2002).

[12] J.M. Serra, E. Guillon, A. Corma, J. Catal. 227 (2004) 459–469.

[13] (a) A. Corma, et al., J. Catal. 189 (2000) 382;
(b) A. Corma, J.M. Triguero, S. Valencia, E. Benazzi, S. Lacombe, J. Catal. 206 (2002) 125–133.

[14] S.-H. Lee, D.-K. Lee, C.-H. Shin, Y.-K. Park, P. Wright, W.M. Lee, S.B. Hong, J. Catal. 215 (2003) 151–170.

[15] M.K. Rubin, US Patent 4,981,663 (1991).

[16] S.I. Zones, L.T. Yuen, S.J. Miller, US Patent 6,709,644 (2004).

[17] J.L. Schlenker, W.J. Rohrbaugh, P. Chu, E.W. Valyocsik, G.T. Kokotailo, Zeolites 5 (1985) 355–358.

[18] S.I. Zones, A.W. Burton, J. Mater. Chem. 15 (2005) 4215–4223.

[19] (a) P. Wagner, S.I. Zones, R.C. Medrud, M.E. Davis, Angew. Chem. Int. Ed. 38 (1999) 1269;
(b) J.L. Casci, B.M. Lowe, T.V. Whittam, in: Proc. 6th Int. Zeolite Conf., Butterworths, Reno, 1983, p. 894.

[20] R.F. Lobo, M. Tsapatsis, C.C. Freyhardt, I.Y. Chan, C.Y. Chen, S.I. Zones, M.E. Davis, J. Am. Chem. Soc. 119 (1997) 3732–3744.

[21] C.Y. Chen, L.W. Finger, R.C. Medrud, P. Crozier, I.Y. Chan, T.V. Harris, S.I. Zones, Chem. Commun. (1995) 1775–1776.

[22] R.F. Lobo, M. Tsapatsis, C.C. Freyhardt, S. Khodabandeh, P. Wagner, K.J. Balkus, C.Y. Chen, S.I. Zones, M.E. Davis, J. Am. Chem. Soc. 119 (1997) 8474–8484.

[23] (a) A. Corma, M. Diaz-Cabanas, F. Rey, S. Nicolopoulus, K. Boulahya, Chem. Commun. (2004) 1356–1357;
(b) B. Harbuzaru, J. Paillaud, J. Pataran, N. Bats, Science 304 (2004) 990–992.

[24] A. Corma, M.J. Diaz-Cabanas, J.L. Jorda, C. Martinez, M. Moliner, Nature 443 (2006) 757–758.

[25] C.Y. Chen, S.I. Zones, L.M. Bull, S.-J. Hwang, in: Proc. 14th Int. Zeolite Conf., IZA, 2004, p. 1547.
[26] S.I. Zones, S.-J. Hwang, Microporous Mesoporous Mater. 58 (2003) 263.
[27] S.I. Zones, A. Rainis, T.V. Harris, D.S. Santilli, US Patent 5,106,801 (1992).
[28] Y. Nakagawa, C.B. Dartt, US Patent 5,968,474 (1999).
[29] S.A. Elomari, US Patent 6,555,089 (2003).
[30] Y. Nakagawa, US Patent 5,316,753 (1994).
[31] S.I. Zones, S.-J. Hwang, Chem. Mater. 14 (2002) 313–320.
[32] Y. Nakagawa, in: J. Weitkamp, W. Holderich (Eds.), Proc. 10th Int. Zeolite Conf., vol. 84, Elsevier, Amsterdam, 1994, pp. 323–330.
[33] I.Y. Chan, P. Laban, P. Crozier, S.I. Zones, Microporous Mater. 3 (1995) 409.
[34] C.Y. Chen, L.W. Finger, R.C. Medrud, C.L. Kibby, P.A. Crozier, I.Y. Chan, T.V. Harris, L.W. Beck, S.I. Zones, Chem. Eur. J. 4 (7) (1998) 1312–1323.
[35] S.I. Zones, C.Y. Chen, K. Balkus, in: M. Occelli, H. Kessler (Eds.), Zeolite Materials, Plenum, New York, 1995.
[36] L.T. Yuen, S.I. Zones, T.V. Harris, A. Aroux, E. Gallegos, Microporous Mater. 2 (1994) 105.
[37] S.I. Zones, T.V. Harris, Microporous Mesoporous Mater. 35–36 (2000) 31–46.
[38] A. Corma, M.E. Davis, Chem. Phys. Chem. 5 (2004) 304–313.
[39] M.E. Davis, S.I. Zones, in: M. Occelli, H. Kessler (Eds.), Synthesis of Porous Materials, Marcel Dekker, New York, 1997, pp. 1–37.
[40] K.J. Balkus, A. Gabrielov, S.I. Zones, I.Y. Chan, in: M. Occelli, H. Kessler (Eds.), Synthesis of Porous Materials, Marcel Dekker, New York, 1997.
[41] S.I. Zones, Y. Nakagawa, J.W. Rosenthal, Zeoraito 11 (1994) 81–90.
[42] S.I. Zones, R.J. Darton, R.E. Morris, S.-J. Hwang, J. Phys. Chem. B 109 (2005) 652–661.
[43] S.I. Zones, Y. Nakagawa, L.T. Yuen, T.V. Harris, J. Am. Chem. Soc. 118 (1996) 7558–7567.
[44] M.D. Shannon, J.L. Casci, P.A. Cox, S.J. Andrews, Nature 353 (1991) 417.
[45] S.I. Zones, A.W. Burton, J. Mater. Chem. 15 (2005) 4215–4223.
[46] R.F. Lobo, S.I. Zones, R.C. Medrud, Chem. Mater. 8 (1996) 2409.
[47] J.L. Casci, P.A. Cox, R.P.G. Henney, S. Maberly, M.D. Shannon, in: Proc. 14th Int. Zeolite Conf., 2004, p. 110–117.
[48] S.B. Hong, E.G. Lear, P.A. Wright, W. Zhou, P.A. Cox, C.-H. Shin, J.-H. Park, I.-S. Nam, J. Am. Chem. Soc. 126 (2004) 5817–5826.
[49] A.W. Burton, S.A. Elomari, R.C. Medrud, I.Y. Chan, C.Y. Chen, L.M. Bull, E. Vittoratos, J. Am. Chem. Soc. 125 (2003) 1633–1642.
[50] S.L. Lawton, M.E. Leonowicz, R.D. Partridge, P. Chu, M.K. Rubin, Microporous Mesoporous Mater. 23 (1998) 109.
[51] C.Y. Chen, S.I. Zones, A.W. Burton, Microporous Mesoporous Mater. (2007), in press.
[52] L.T. Yuen, J.S. Geilfuss, S.I. Zones, Microporous Mater. 12 (1997) 229–249.
[53] M.F.M. Post, J. van Amstel, H.W. Kouwenhoven, in: D. Olsen, A. Attilio (Eds.), Proc. of the 6th Int. Zeolite Conf., Butterworths, MA, USA, 1983, p. 517.
[54] C.D. Chang, Hydrocarbons from Methanol, Academic Press.
[55] J.F. Haw, J.B. Nicholas, W. Song, F. Deng, Z. Wang, T. Xu, C.S. Heneghan, J. Am. Chem. Soc. 122 (2000) 4763–4775.
[56] S. Svelle, F. Joensen, J. Nerlov, U. Olsbye, K.-P. Lillerud, S. Kolboe, M. Bjorgen, J. Am. Chem. Soc. 128 (2006) 14770–14771.
[57] J. Weitkamp, S. Ernst, R. Kumar, Appl. Catal. 27 (1986) 207.
[58] J.V. Cejka, A. Krejc, N.V. Zilkova, J. Kotrla, S. Ernst, A. Weber, Microporous Mesoporous Mater. 53 (2) (2002) 121–133.
[59] V.J. Frillette, W.O. Haag, R.M. Lago, J. Catal. 67 (1991) 211.
[60] C.W. Jones, S.I. Zones, M.E. Davis, Appl. Catal. A Gen. 181 (1999) 289–303.
[61] C. Baerlocher, F. Gramm, L. Massueger, L.B. McCusker, Z.B. He, S. Hovmoller, X.D. Zou, Science 315 (2007) 1113–1116.